ACTIVITIES ON RF-SUPERCONDUCTIVITY AT WUPPERTAL

H. Heinrichs, G. Arnolds-Mayer *), T. Grundey,
U. Klein**), N. Minatti, G. Müller, M. Peiniger,
H. Piel, G. Unterbörsch, H.P. Vogel

Bergische Universität-Gesamthochschule Wuppertal
Fachbereich 8, Physik, Gaußstr. 20
5600 Wuppertal 1

*) now Associate at CERN

**) now at Interatom GmbH., Bensberg

Presented by H.Heinrichs

The main activities in rf superconductivity at the University of Wuppertal today are the construction of the superconducting recyclotron at Darmstadt together with the Institut für Kernphysik der Technischen Hochschule Darmstadt (TH), the analysis of field and Q limitations and the development of Nb_3Sn coated structures which would open the possibility to operate an accelerator at a temperature of 4.2 K even at frequencies above 1 GHz. Moreover we concentrate upon the determination of fundamental parameters of superconductors, like the surface resistance and its temperature dependence at 20 to 26 GHz and at 80 to 86 GHz.

I. The Superconducting Recyclotron of the Darmstadt Wuppertal Collaboration

1. General Layout

The superconducting recyclotron is described in [1]. I shall restrict myself to a report on the present state.

The project was granted in the beginning of 1983. The new buildings at the TH Darmstadt are almost completed. The superconducting recyclotron operating at 3 GHz is designed to accelerate a c.w. electron beam to 130 MeV with an energy spread of 10^{-4}. The general layout is shown in Fig. 1. An electron gun (Dowlish Developments) accelerates a beam of up to 2 mA to max. 300 keV with an energy stability of 10^{-4}. A chopper and prebuncher system will match the phase space so that the electron beam has a bunch length of 1.1 Deg. and an energy spread of ± 6 keV when it leaves the injector, i.e. when it is accelerated by a 5 cell structure (E_{acc} = 6 MV/m) and two 20 cell structures (E_{acc} = 5 MV/m) to at least 11 MeV. [2] The beam is then bent isochronously by 180° and injected into a linear accelerator consisting of eight one meter long structures with a design accelerating

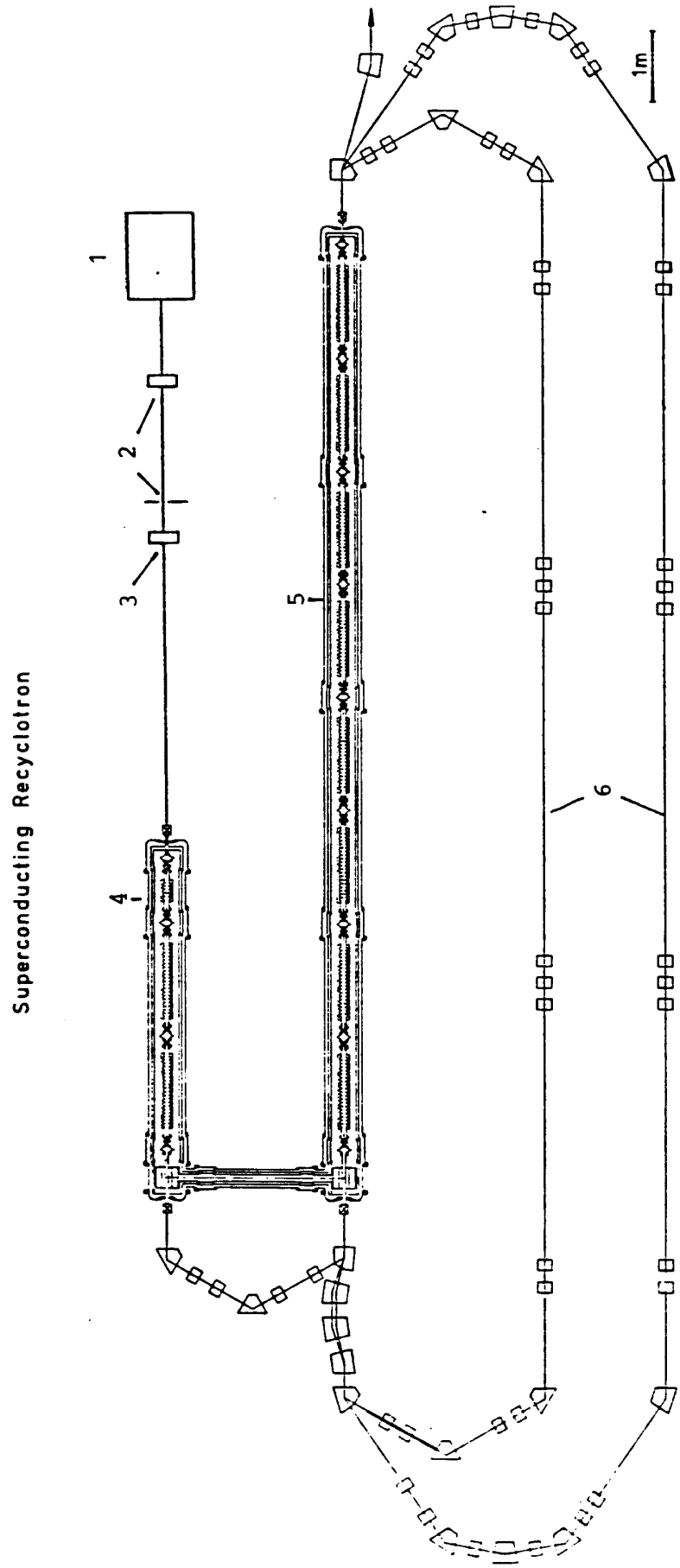

Fig. 1: General layout of the superconducting recyclotron
1 Electron Gun, 300 KV, 2 Chopper, 3 Prebuncher,
4 Injector, 5 Linac, 6 Recirculation system

field of 5 MV/m. To reach a final energy of 130 MV the beam is recycled twice through this linear accelerator. The parameters of the recyclotron are given in table 1. The construction will happen in three steps: building up and operation of the injector (and the whole cryogenic system) with a maximum energy of 11 MeV, completion of the linear accelerator with its 8 superconducting structures, installation of the recirculation system.

All room temperature components of the recyclotron are designed and constructed by the TH Darmstadt. The cryogenic system and the superconducting accelerating structures are our contributions to this accelerator.

2. Cryogenic System

The cryogenic system consists of a refrigerator including transfer line and a modular constructed cryostat. The refrigerator (Gebrüder Sulzer AG, Winterthur, Switzerland) has an output power of 100 W at 2 K. It can operate in a refrigeration as well as in a liquefying mode. The pressure in the cryostat is designed to be constant within ± 1 mbar, the liquid helium level within ± 10 mm. The first operation will be next month (Aug. 1984). The cryostat, designed at Wuppertal and manufactured at Arthur Pfeiffer, Vacuumtechnik GmbH, Aßlar, is constructed in a modular way so that an exchange of structures is easily possible. It consists of five accelerator moduls, each houses two one meter structures. This modul is shown in Fig. 2. It is designed as a bath cryostat with a liquid nitrogen radiation shield. This guarantees a more safe operation of the cryostat system because it is not necessary to warm up the whole cryostat to room temperature during shut down times. The vacuum jacket and the helium vessel are made from stainless steel (1.4301 resp. 1.4429 to avoid magnetisation), the radiation shield is fabricated from aluminium. All helium vessels are connected to one another. This construction minimizes heat losses and the

Table 1: Parameters of the recyclotron

General	
max. energy	130 MeV
min. energy	6 MeV
energy spread	±13 KeV
max. beam current	20 μA
duty cycle	1 (c.w.)
operation temperature	2 K
Structures	
frequency	2997.9 MHz
mode	π
effective (total) length	1. (1.3) m
number of cells	20
Q-value at 2 K	$3 \cdot 10^9$
accelerating field	5 MV/m
dissipated power	4.1 W/m
Injector	
gun voltage	250 KV
voltage stability	10^{-4}
current of the gun	1 mA
structures: 2 20 cell (1 m)	1 5 cell (.25 m)
max.energy	11 MeV
energy spread	±6 KeV
Linac	
structures: 8 20 cell (1 m)	
ratio total length to effective length	1.9
energy gain	40 MeV
max. current (incl. two recirculated beams)	60 μA
Cryogenic system	
length of injector cryostat	5.9 m
length of linac cryostat	15.1 m
diameter of helium vessel	.25 m
liquid helium in the cryostat	600 l
standby losses	25-35 W
consumption of LN_2	10-15 l/h
refrigerator power at 2 K	100 W

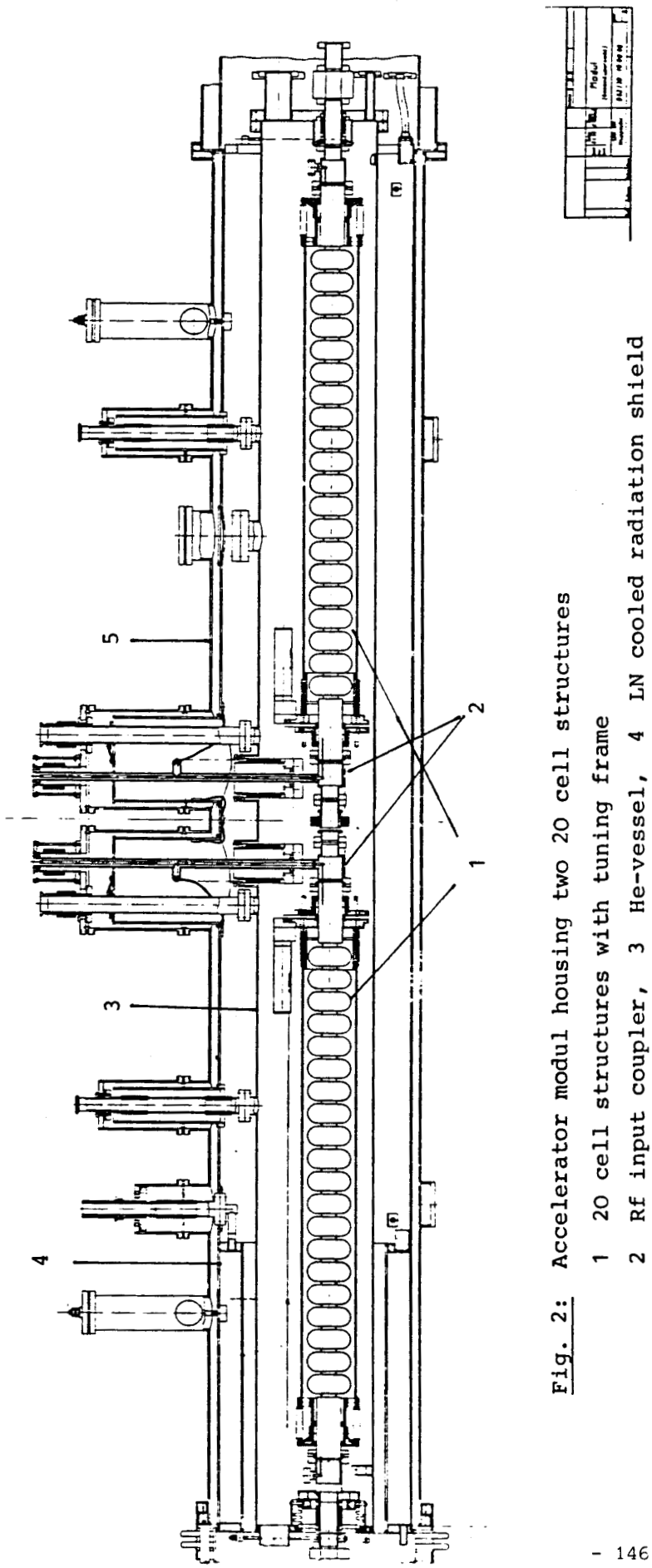

Fig. 2: Accelerator modul housing two 20 cell structures

1 20 cell structures with tuning frame

2 Rf input coupler, 3 He-vessel, 4 LN cooled radiation shield

5 Vacuum tank

standby losses of the whole 23 m long system are expected to be about 25 Watts. All cold parts are superisolated. The minimization of heat losses also requires that the whole cryostat is housed in one vacuum system. Before mounting the whole system each modul can be vacuum tested. All cold flanges are of conflat type, copper sealed, only connections from the cavity to the beam tube (niobium to stainless steel) are sealed with indium. Flange connections between the beam vacuum and the liquid helium bath are avoided if ever possible.

3. Structure design, construction and tests

The s.c. accelerating structures to be used in the recyclotron are a five cell structure as a capture section and ten one meter long 20-cell structures. All structures are velocity of light structures. Fig. 3a shows a cross sectional view of the five cell structure with the coupling probe mounted in a tuning frame, Fig. 3b shows a photo of the 20 cell structure. Table 2 summarizes characteristic parameters of the structures.

The structures are designed to operate at 2997.9 MHz in the π-mode. Each cell has a spherical shape to suppress multipacting. The opening at the iris has a diameter of 35 mm.

Table 2: Parameters of the structure (20 cell)

reduced shunt impedance	2010	Ω/m
geometrical factor	293	Ω
E_{peak}/E_{acc}	3.0	
H_{peak}/E_{acc}	41,8	Oe/(MV/m)
$E_{acc}/\sqrt{PQ}$	$4.5 \cdot 10^{-5}$	MV/m/$\sqrt{W}$
cell coupling coefficient	4	%

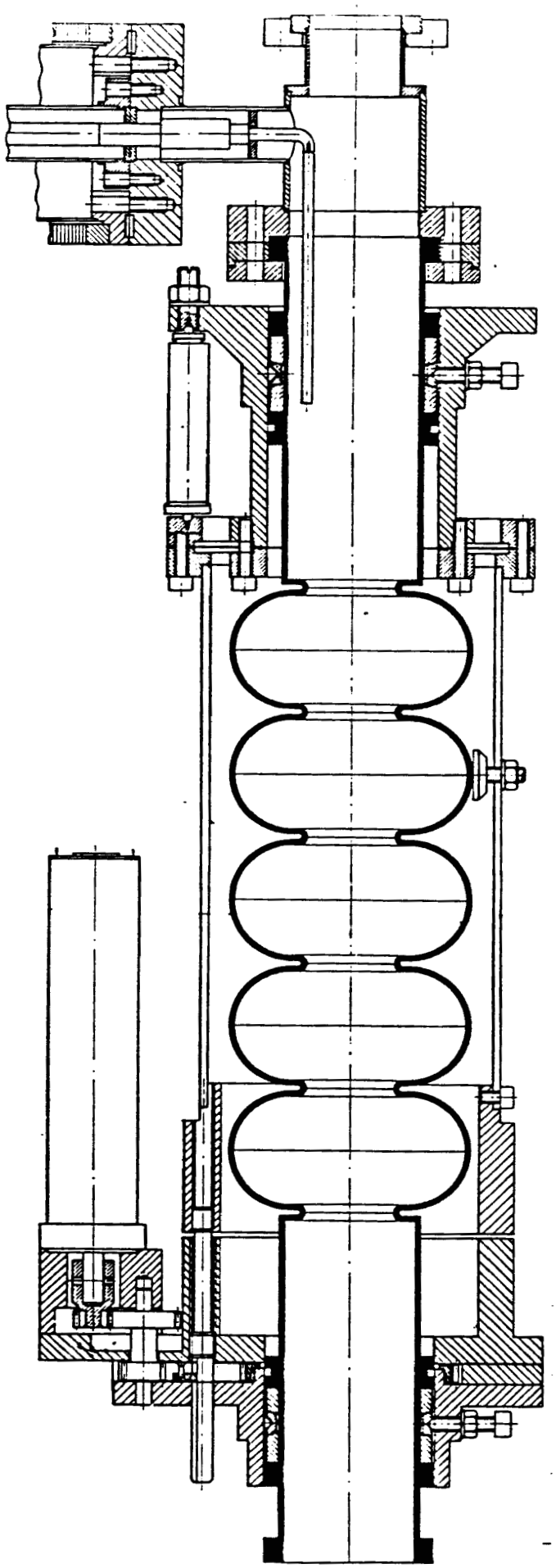

Fig. 3a: Five cell structure (capture section) with tuning support and coupling.
Left side:motor driven coarse tuner
Right side: piezoelectrically driven fine tuner

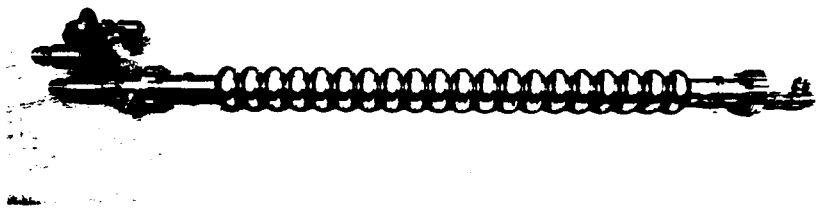

Fig. 3b: Photo of the 20 cell structure

The cell to cell coupling is about 4 %. The diameter of the end cells (Ø 89.34 mm) is smaller than that of the middle cells (Ø 90.06 mm) to correct the influence of the cut off tube. The diamter of the cut off tube is 50 mm and has been chosen for a free propagation of the TM 110 mode. It propagates all dipol modes exited inside the structure for frequencies above 3.5 GHz and all monopol modes with the exception of the fundamental mode. The microwave power is fed into the structure via a demountable antenna in the cut off tube. The coupling coefficient can be adjusted by the length of the antenna.

The structures are fabricated from 2 mm niobium sheet metal. Each sheet is inspected after a 5 µm chemical polishing. That side of the sheet which shows less visible defects, (scratches, pits etc.) is defined to become the inner side of the cell. Then the sheets are deep drawn to the form of a half cell. Next each cup is stress annealed before cutting the ring with which the sheet metal is held during the deep drawing. Before welding of two cups each cup is again inspected and visible defects are ground. Anodizing to a light yellow or dark blue colour is used to find defects and impurities. Welding edges are chemically polished (10 µm), and within two days the cups are welded to give a cell. The equatorial welding seam is carried out first from outside with 80 % penetration then from inside with about 30 % penetration. In all s.c. tests carried out with cavities welded in this way we never found a quench located on the equatorial welding seam.

In this stage all cells are frequency tuned by chemical polishing to the design frequency. Each cell has to be tuned by a different amount to reduce the frequency band width of all cells from about 3 MHz caused by productional tolerances to about 200 KHz after tuning. The end cells are prepared in the same way. After machining of the welding edges twenty cells are stacked together to form a 20 cell structure and the field distribution is measured. Although the coupling coefficient from cell to cell is quite large (4 %) the π-mode of the structure is not separated well from its nearest lower pass band mode because of the low Q-value of 6000 at room temperature. This $19\pi/20$ mode shows a high exitation of the end cells, but it has zero excitation in the middle cell of the structure. To suppress the admixture of this mode to the π-mode we put a further cell in the middle of the chain of the 20 cell structure - to form a 21 cell structure - and excite the structure by coupling the rf-power into this middle cell. In this arrangement the contribution to the π-mode field distribution due to the admixture of other modes is less than the accuracy of the bead pull measurement. [3]

After finding the flat field distribution the structure is welded at the irises. This welding is carried out from the outside. Because of the narrow slit between two cells and the small curvature at the irises it is very difficult to do the welding so that the inner surface becomes smooth. In the past it was often necessary to grind the welding seam from inside. As a consequence of the high sensitivity of the π-mode against errors in coupling from cell to cell the field distribution became unflat. This unflatness is removed by a slight mechanical deformation of the appropriate cells of the structures.

These steps of construction have been tested with several five cell structures and one 20 cell structure. The production of the structures for the recyclotron has started, the cups are deep drawn and stress annealed. The mechanical working and the EB welding are carried out at Interatom GmbH, Bensberg, the heat and chemical treatment and the rf measurements are done at Wuppertal.

The dynamic frequency tuning at low temperatures is done by changing the length of the structure. As shown in Fig. 3 the tuning system consists of two tuning mechanism: one is a motordriven coarse tuner and the other a piecoelectrically driven fine tuner. Related to a frequency change df per change of length of the structure dl of $\frac{df}{dl} \propto 250 \frac{KHz}{mm}$ for the 20 cell structure the tuning range of the coarse tuner is 1 MHz with a resolution of better than ± 200 Hz. The tuning range of the fine tuner is max. 5 KHz, the resolution is better than .5 Hz. In a first test in which a five cell structure was tuned to the frequency of a single cell cavity it turned out that the structure is very sensitive to accustic vibrations. Nevertheless, the frequency of the five cell structure could be locked. Further experiments are necessary to improve the electronic system of the tuning device.

In more than twenty low temperature tests carried out with five cell structures we could show that the design values of $Q = 3 \cdot 10^9$ and $E_{acc} = 5$ MV/m at 2 K can be reached. Typical values which could be achieved with "standard" preparation are $Q = 4 \cdot 10^9$ and $E_{acc} = 6.5$ MV/m. Here "standard" preparation means a sequence of the following step of treatment: after cleaning in an alkaline bath under ultrasonic agitation the structure is chemically polished in a solution of HF (40 %), HNO_3 (65 %), and H_3PO_4 (89 %) (1:1:1). Since the end of a long structure which enters the acid first will be polished more than the other, the structure is polished

upside down again. Typically 20 to 30 µm are removed. Then the structure is rinsed with demineralized dust free water until the conductivity of the outlet water nearly equals the conductivity of the inlet water. Then the structure is dried in a dust free atmosphere and evacuated. In a first low temperature test defects and regions of enhanced dissipation are localized by temperature mapping. [4] Local grinding of the defect region eventually followed by local chemical polishing is carried out after warm up. The structure then is surface treated as described again and eventually heat treated at 1200°C to 1500°C in a vacuum of 10^{-7} mbar or better as the last step of preparation.

Up to now we have tested one 20 cell structure. In a first low temperature test we reached a Q-value of $Q_o = 10^9$ and an accelerating field of $E_{acc} = 3.7$ MV/m. The temperature "landscape" of the structure measured at $E_{acc} = 2.8$ MV/m is shown in Fig. 4a. The quench occurred in cell 5 near iris 5 (left peak in Fig. 4a). After warm up the structure was inspected with an endoscope. In cell 5 and 9 visible defects were found, but not in cell 19. The visible defects were ground. In the next low temperature test the map shown in Fig. 4b was taken at a field of $E_{acc} = 3.5$ MV/m. The ground defect region disappeared and a new defect on iris 9 was created. But the quench occurred in this test in cell 19 and not in cell 8. This can be seen on temperature maps (or even better on maps showing the heat flux through the cavity wall which can be calculated from these temperature maps, for a detailed analysis see the talk of G. Müller [6]), which were taken at higher fields than 3.5 MV/m. The heat production in cell 19 increased more rapidly than that in cell 8. The quench occurred at a field of $E_{acc} = 4.2$ MV/m. As described above the field distribution of the structure was unflat, the field in the quenching cell was about 5.7 MV/m which also can be deduced from the temperature maps. [6]

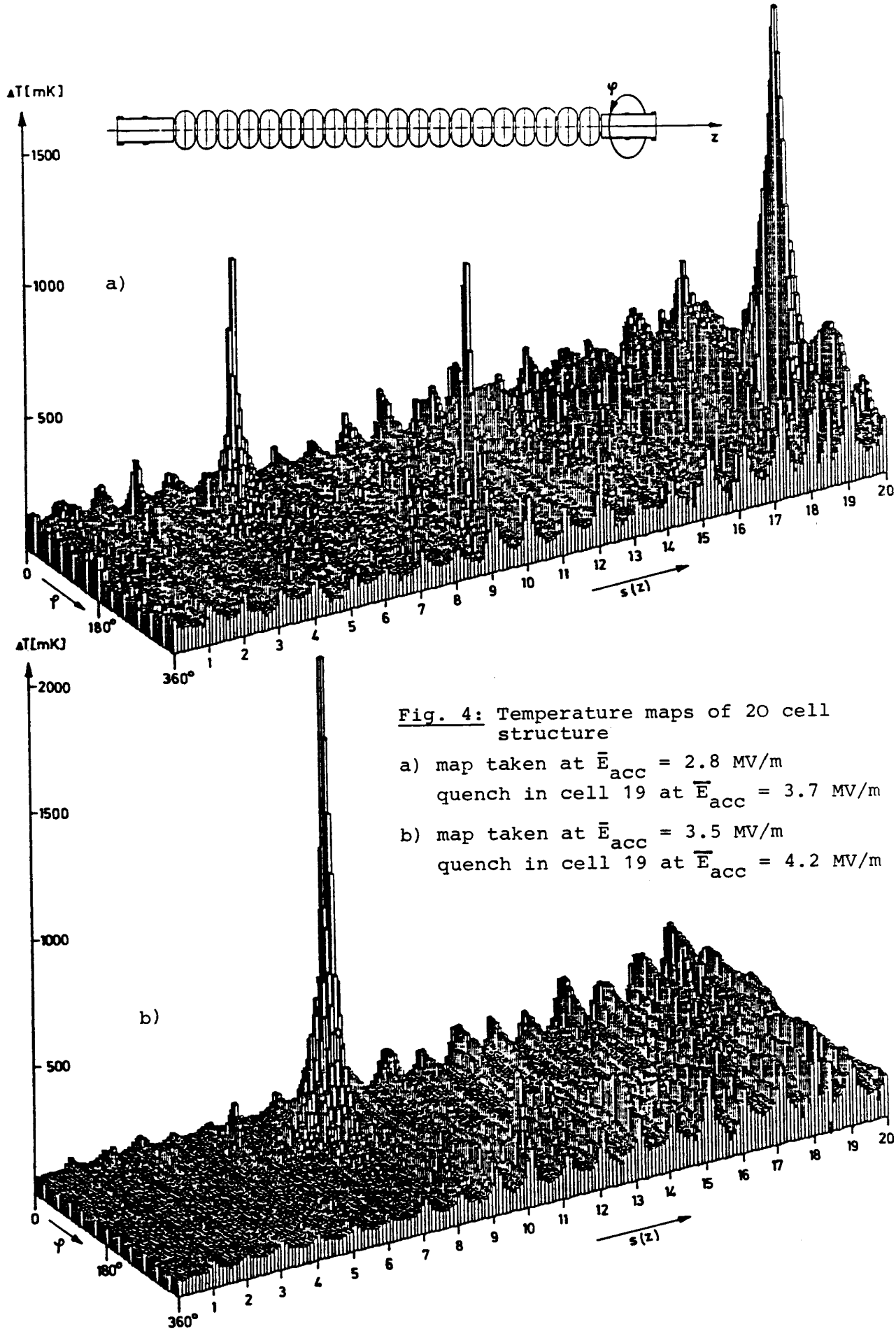

Fig. 4: Temperature maps of 20 cell structure

a) map taken at $\bar{E}_{acc}$ = 2.8 MV/m
quench in cell 19 at $\bar{E}_{acc}$ = 3.7 MV/m

b) map taken at $\bar{E}_{acc}$ = 3.5 MV/m
quench in cell 19 at $\bar{E}_{acc}$ = 4.2 MV/m

All five and 20 cell structures were manufactured from niobium material which had an RRR of less than 40.

4. Pilot Accelerator and Injector Model

To test several components of the superconducting recyclotron we have together with our colleagues of the TH Darmstadt built up and operated a small superconducting linear accelerator which served as a pilot project. [5] The experimental setup is schematically shown in Fig. 5. A 200 KeV continuous electron beam was chopped at 3 GHz by two transverse deflecting rf-cavities and a chopping orifice. With a five cell structure like the capture section of the recyclotron which had a value of $Q = 4 \cdot 10^9$ and an accelerating field of $E_{acc} = 5.7$ MV/m at 1.8 K this beam was

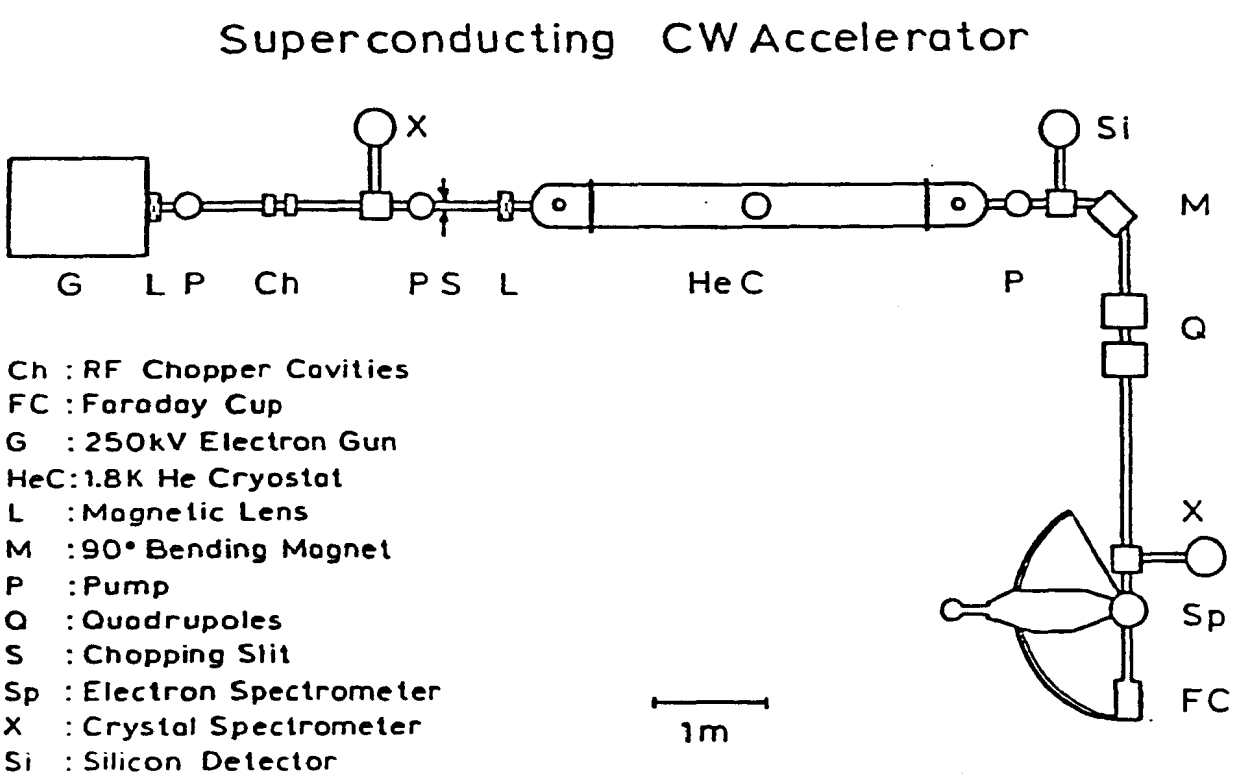

Fig. 5: Experimental setup of pilot accelerator

accelerated to 850 KeV. It was analysed by the spectra of Mott scattered electrons from a carbon foil by a cooled Si-detector. The spectra are shown in Fig. 6.

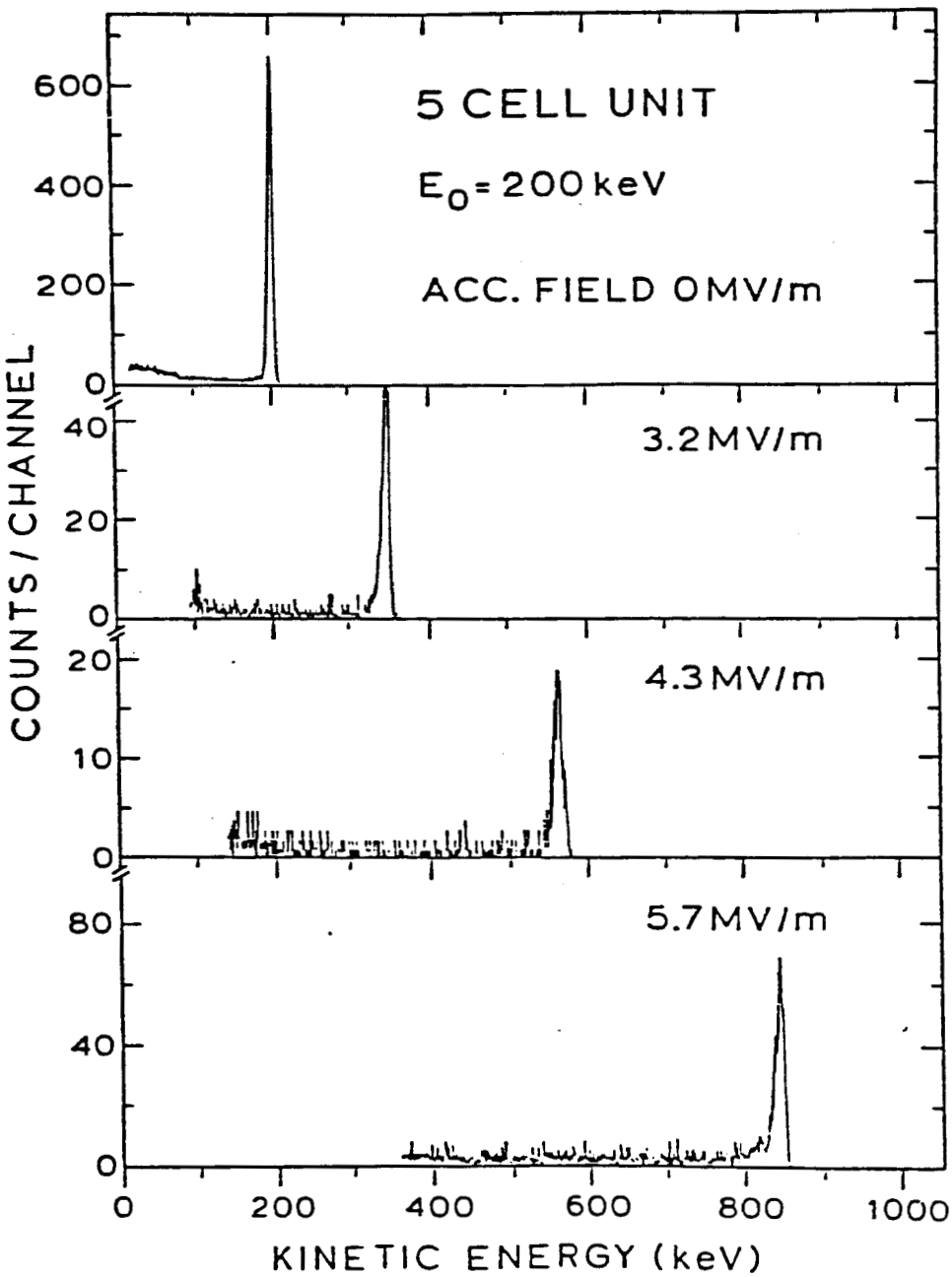

Fig. 6: Energy spectra of Mott-scattered electrons for different accelerating fields

To improve the beam transport system the structure had to be cooled down and warmed up for more than six times during a period of one year. The structure was always kept under vacuum, no deterioration of Q and E_{acc} could be observed. Also all other components of the accelerator including the cryostat performed according to our expectations.

II. Development of Superconducting Structures

The study of the physical nature of field limitations far below theoretical limits is our main subject of research. Until now defects seem to be the most severe problem. A detailed discussion is given in [6].

In order to reach high fields and high Q-values we try to avoid or to remove big defects by clean preparational methods and grinding and to stabilize defect by increasing the thermal conductivity of the niobium. We found that e.g. the use of low conductivity ($\leq$ 18 MΩ cm) demineralized water during the last step of preparation is essential to reach high Q-values. The lower the conductivity of the rinsing water when it leaves the structure the higher the Q-values we reached, $Q_o = 3 \cdot 10^9$ to $1 \cdot 10^{10}$ in a 3 GHz single cell cavity. The highest Q-value, $Q_o = 7 \cdot 10^{10}$, we reached after bake out at 1800°C. The maximum accelerating field was independent of the Q-value and could be increased by grinding typically to $E_{acc} \sim 7$ MV/m, once we reached 10 MV/m. [7] All these data were taken from cavities fabricated from niobium with an RRR less than 40 (the RRR of the cavity with which we reached 10 MV/m is unknown).

Since W.C.Heraeus GmbH., Hanau has refined its production process and sheet metal with an RRR of 80 to 135 could be produced the maximum accelerating field in cavities fabricated from this material increased at least by a factor of two.

We have built two single cell cavities, one from the RRR = 80-material and one from the RRR = 135-material. In the first one we reached a field of E_{acc} = 12 MV/m and Q = 3.10^9 at this field level. The field was limited by quenching. In the second cavity we could reach fields up to E_{acc} = 16.3 MV/m without quenching. We could not get up higher because of large field emission currents and the available rf-power. Fig. 7 shows

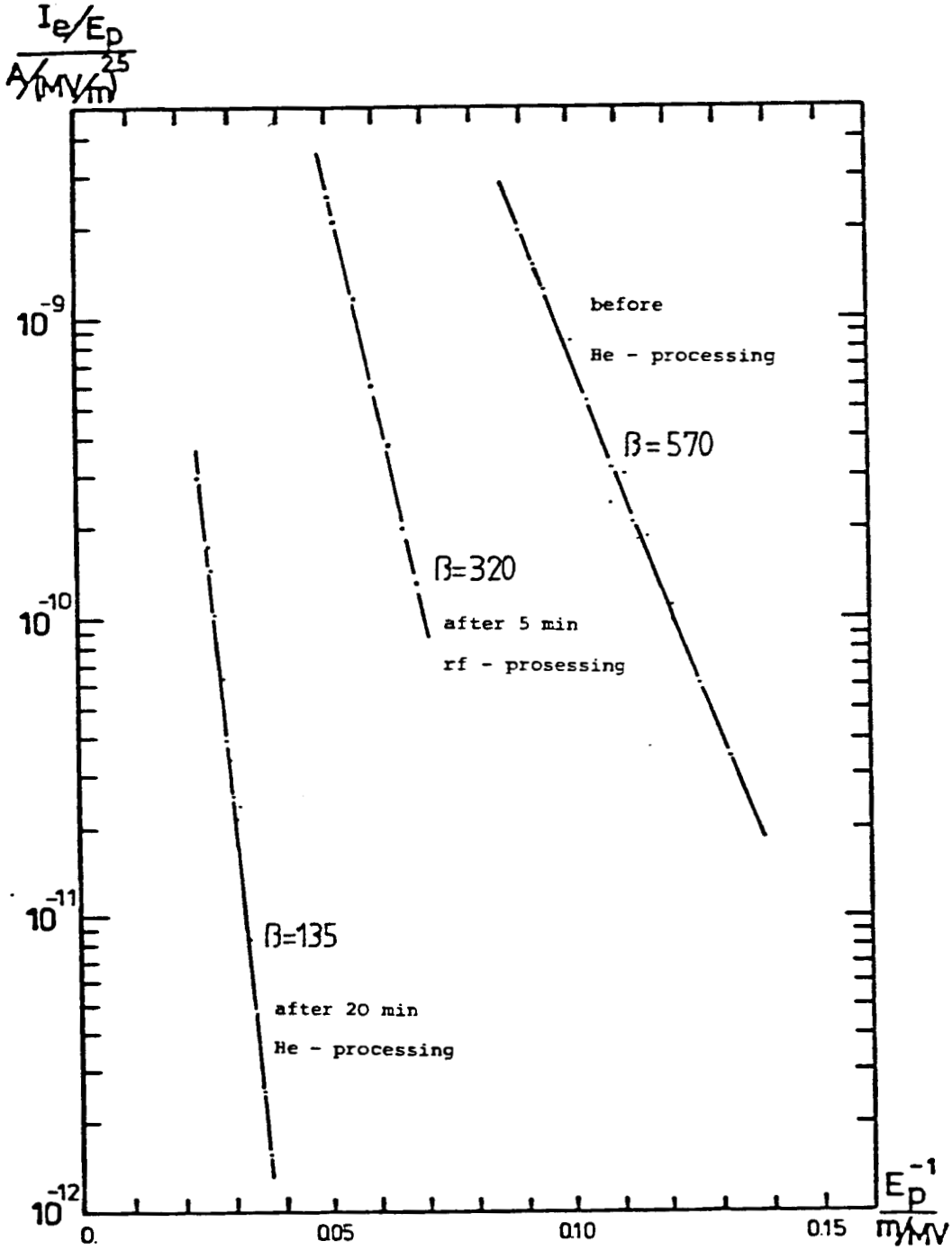

Fig. 7: Fowler-Nordheim plot of field emitted electron current measured in a cavity fabricated from high thermal conducting niobium at fields up to E_{acc} = 16.3 MV/m

a Fowler Nordheim plot of the field emitted current during this test. It was measured with a pick up probe in the cut off tube. Increasing the field for the first time we measured a F.N. field enhancement factor β of 570, after 5 min.rf-processing β decreased to 320 and after 20 min. He-processing β again decreased to 135. Because of the insufficient radiation protection a long term He-processing is not yet possible. Fig. 8 shows the corresponding dependence of $Q\ (E_{acc})$.

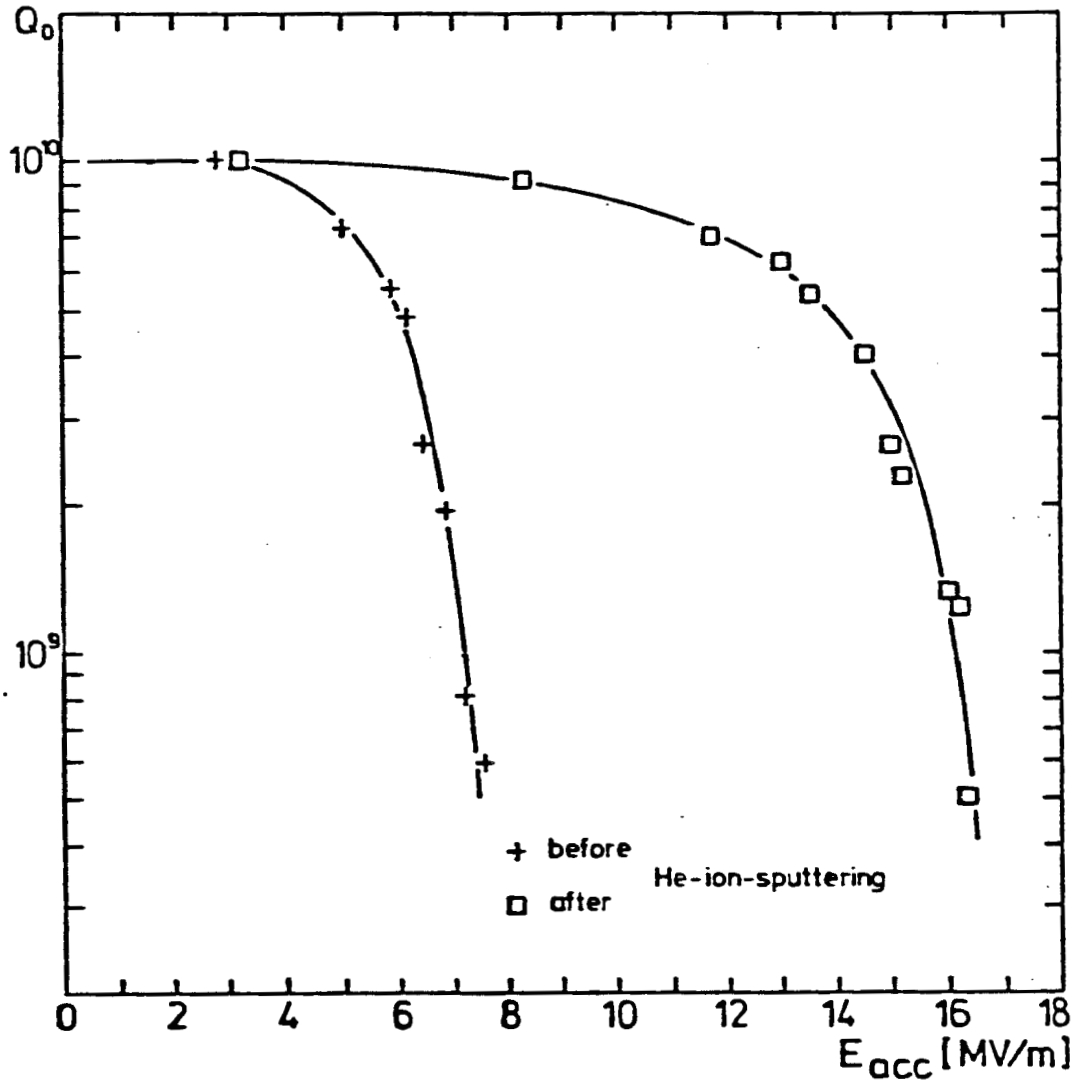

Fig. 8: $Q\ (E_{acc})$ measured in a cavity fabricated from RRR = 135 material

Fig. 9 summarizes the maximum achieved accelerating fields as a function of RRR. It shows that E_{acc} increases with increasing RRR, different values of E_{acc} for the same RRR may be due to different sizes of defects. The temperature dependence of the thermal conductivity of the niobium for different RRR is shown in Fig. 10. In addition Fig. 10 shows the thermal conductivity of a probe of the RRR = 80-material which was fired at 1900°C under UHV-conditions. This is characterized by an increase of the thermal conductivity near 2 K due to the phonon peak. We are now investigating the possibility to increase thermal conductivity in the range from 2 K to 5 K.

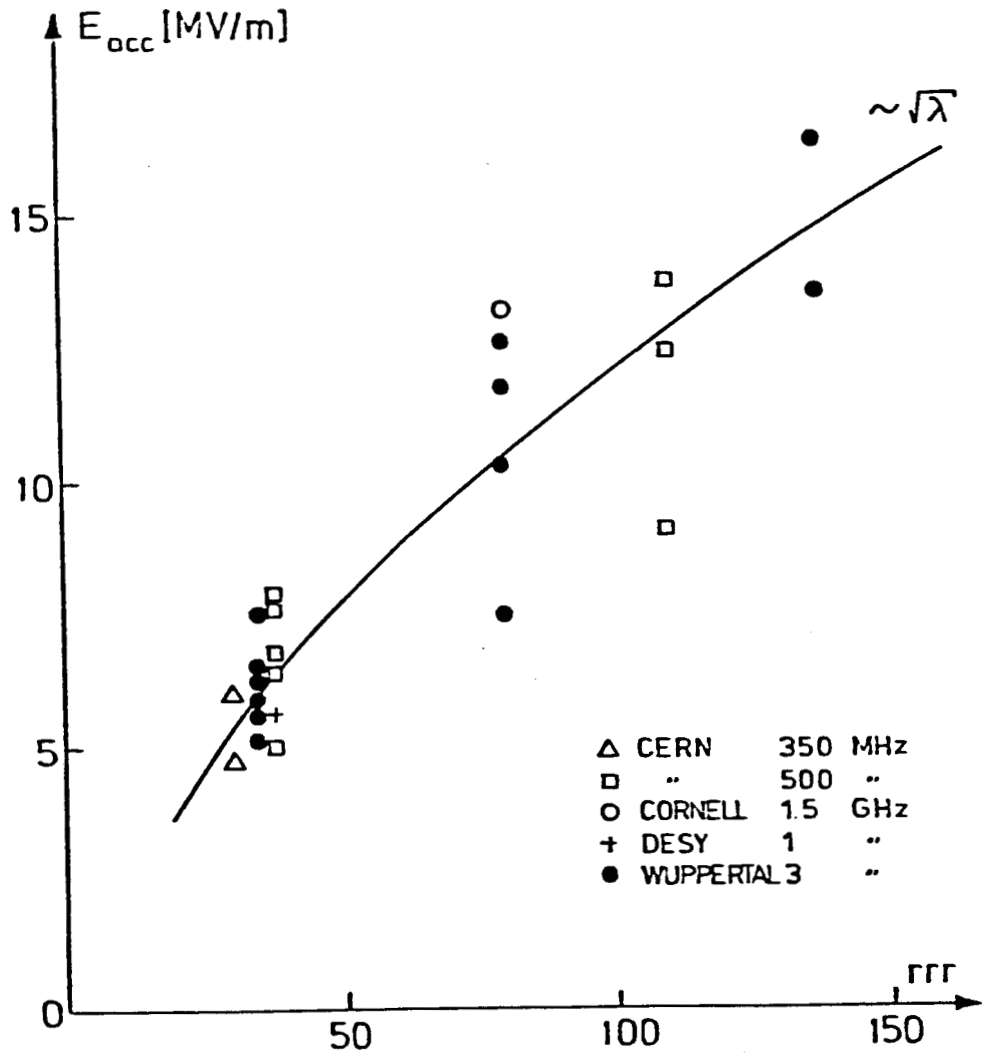

Fig. 9: Maximum achieved accelerating fields in cavities fabricated from material of different RRR

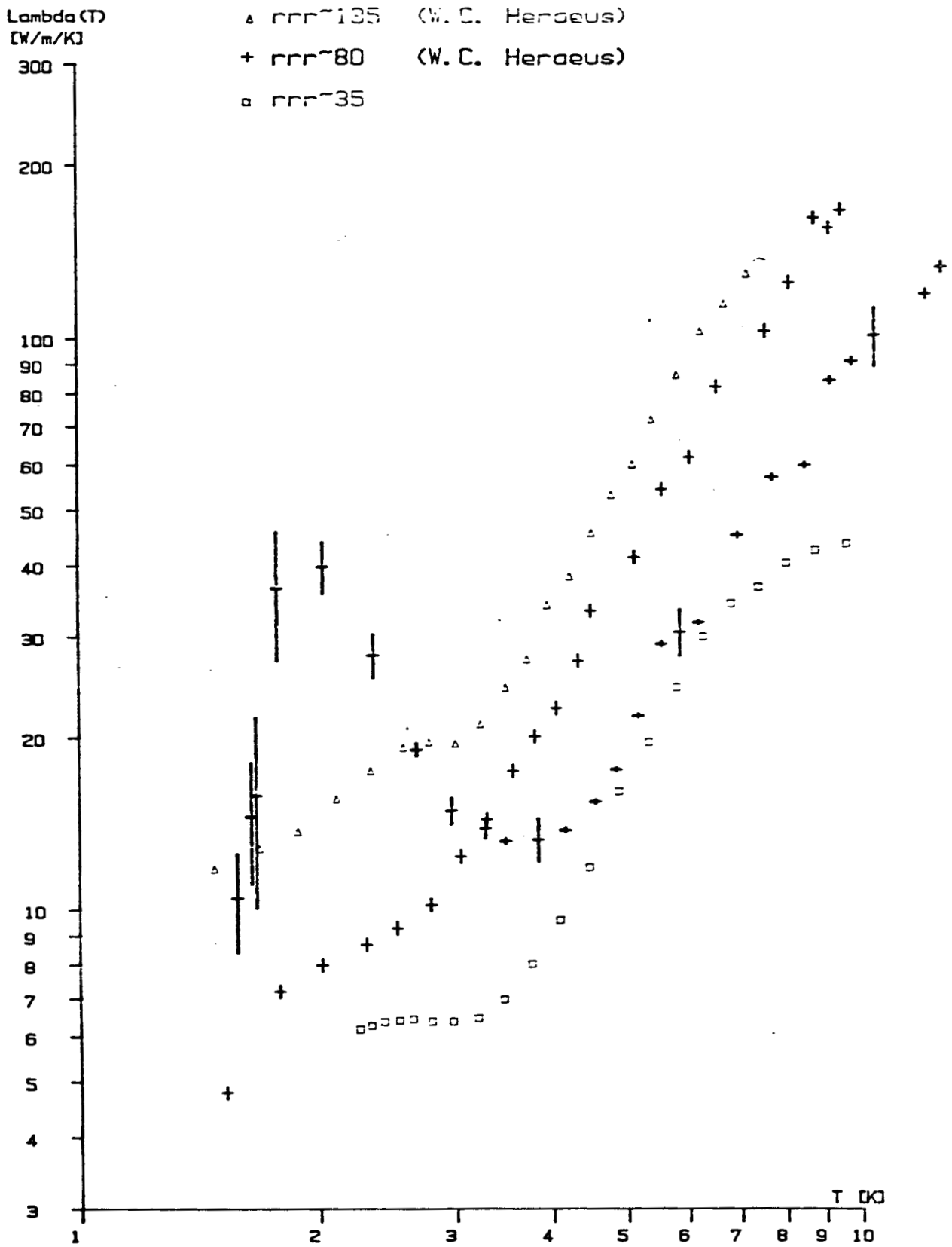

Fig. 10: Temperature dependence of the thermal conductivity of the niobium for different RRR

The fact that we were limited at field level of 16 MV/m by electron loading due to field emission and not by quenching possibly demonstrates that field emission may be the next limiting phenomenon.

III. Nb_3Sn structures

The possibility to operate a superconducting accelerator at a temperature of 4.2 K would reduce the cost of the cryogenic system. Therefore, we study the rf-properties of superconducting Nb_3Sn surfaces in multicell accelerator structures.

The Nb_3Sn layer (about 3-5 μm thick) is produced by vapor deposition of tin on a Nb surface in a furnace at about 1150°C. Normally a thin surface layer of about 1 μm is taken away by oxi-polishing before testing. Fig. 11 shows the temperature dependence of the surface resistance of a Nb_3Sn single cell cavity operated at 3 GHz. [8] In the temperature range from 9 K to 4.2 K (fit 1) one can see the exponential decrease of R_s with an energy gap Δ_o/kT_c = 2.2. Below 4.2 K R_s decreases further to a residual resistance of 55 nΩ corresponding to a Q value of $Q_o = 5 \cdot 10^9$. Fig. 12 shows the Q as a function of the accelerating field: Curve 1 was measured after the first (fast) cool down. These data can be reproduced until the cavity is warmed up above T_c. Curve 2 was measured after the cavity was warmed up above T_c and again cooled down but very slowly (i.e. about 1 K per 10 min.) near T_c. Then the cavity was warmed up again and cooled down (fast) for a third time. The cavity behaved as shown in curve 1. The physical reason for this different behaviour is up to now not clear (frozen magnetic flux due to thermal electric currents ?).

The maximum accelerating field we reached in a 3 GHz single cell cavity is $E_{acc} \approx 7.4$ MV/m at $Q = 7 \cdot 10^8$ in the temperature

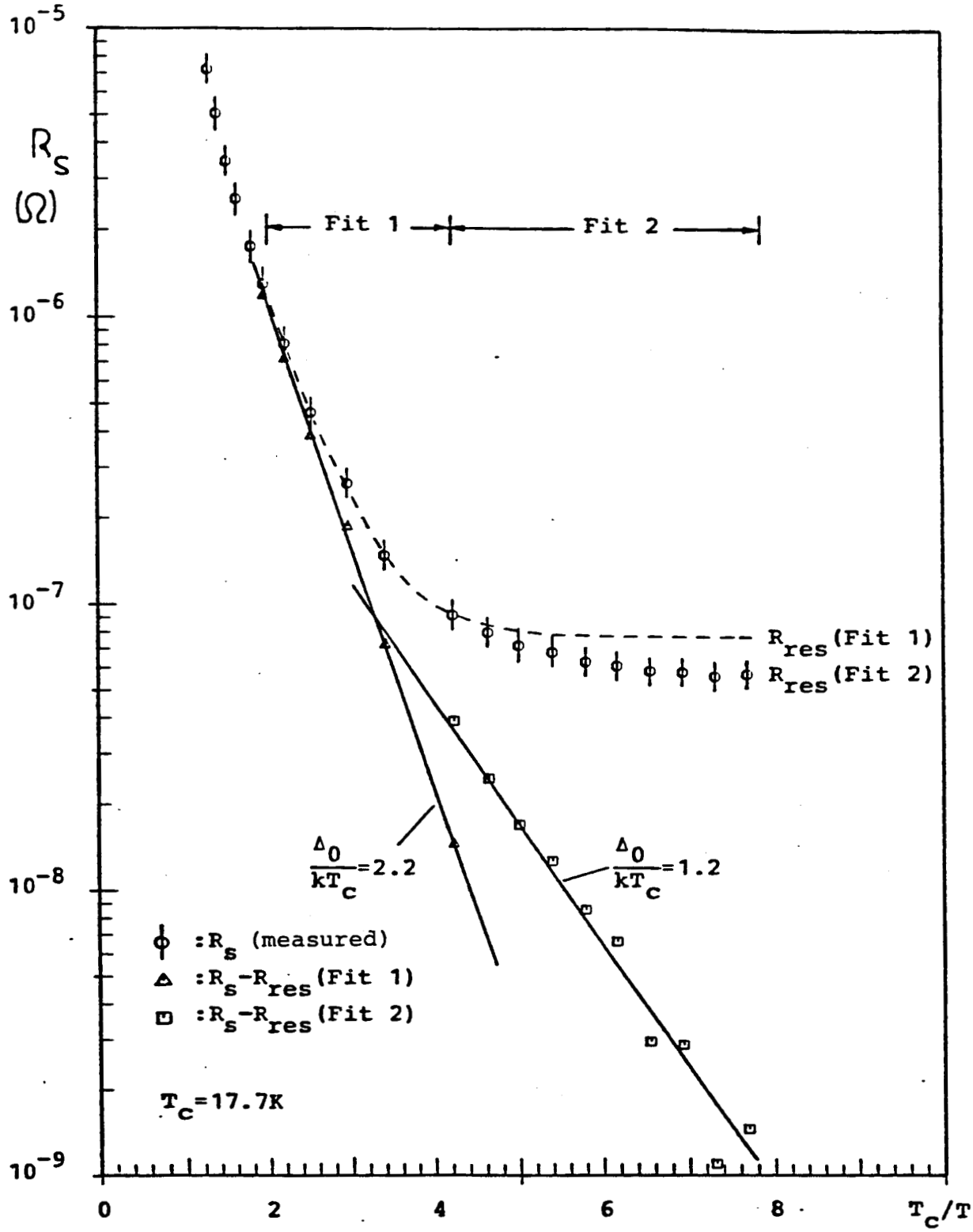

Fig. 11: Temperature dependence of R_s of Nb_3Sn measured in a 3 GHz cavity. Fit 1 fits the data in the temperature range from 9 K to 4.2 K, R_{res} and Δ_o/kT_c are free parameters. Fit 2 fits the data below 4.2 K, respectively.

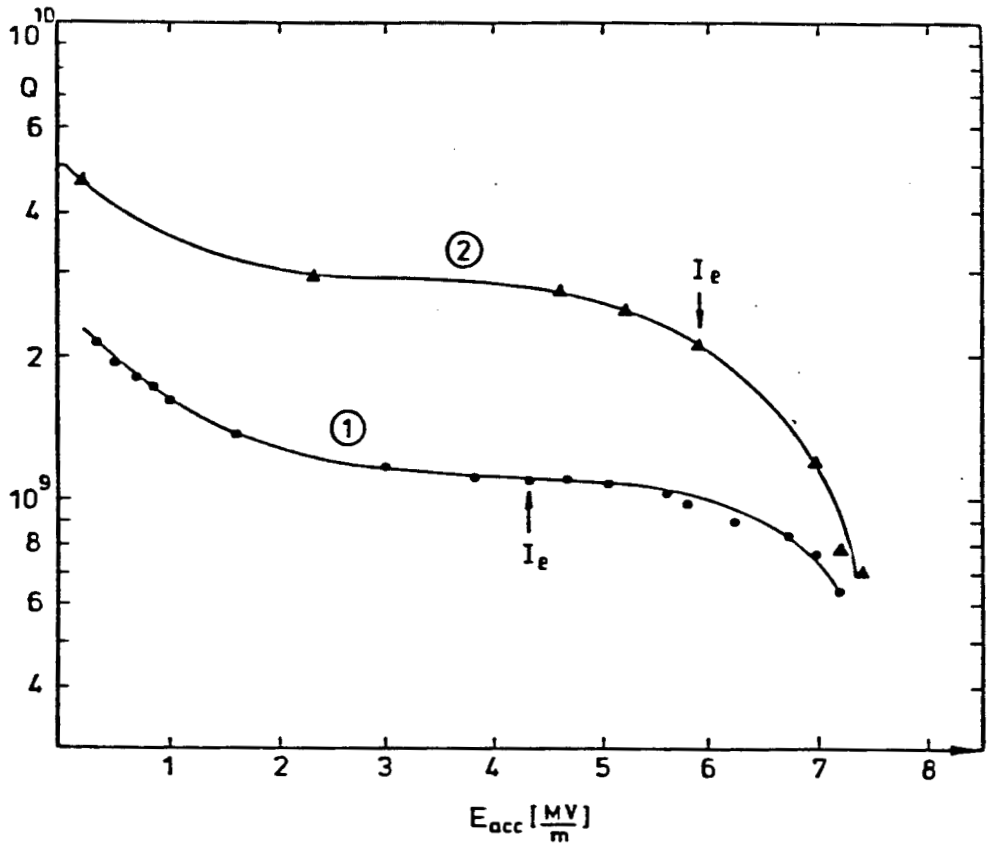

Fig. 12: Q (E_{acc}) of a Nb_3Sn cavity operated at 3 GHz Curve 1 shows the behaviour after a "fast" cool down near T_c , Curve 2 after a slow cool down

range from 4.2 K to 2 K, independent of temperature. The field was limited by quenching, electron loading was observed at field levels as indicated in Fig. 12.

The preparation of a 5 cell Nb_3Sn structure is under way. Moreover it is planned to develop a single cell cavity as well as a three cell structure at a frequency of 1 GHz.

A detailed discussion on Nb_3Sn surfaces is given by G. Arnolds-Mayer. [9]

IV. Rf-superconductivity at high frequencies

The surface resistance and its temperature dependence in the frequency ranges of 20 to 26 GHz and 83 to 88 GHz were

measured for TE- and TM-mode in pill-box cavities. [10] Fig. 13 shows the experimental setup for the 80 GHz measurements. Because of the high attenuation of the wavequides at these frequencies the microwave power was fed through the bottom of the cryostat, in the 20 GHz setup it was possible to feed the power from the top. Frequency generator was a YIG-tuned gun oszillator (20 GHz) or an Impatt oszillator (80 GHz), respectively.

The temperature dependence of the surface resistance was measured in the range from 4.2 K to 1.4 K. In the TE_{121}-mode of a welded pill-box cavity a maximum Q_o (21.5 GHz, 1.4 K) of $4 \cdot 10^{10}$ was reached, corresponding to a residual resistance below 3 nΩ ($Q_{res} > 3 \cdot 10^{11}$). This value is of the order of the lowest residual resistance reached in niobium cavities at low frequencies. At 80 GHz the lowest residual resistance which was reached was 485 nΩ and only determined by the difficulty of cleaning this very small cavity on its inside. The measurements of temperature dependence of the surface resistance is a test for theories of superconductivity. Fitting the experimental data with BCS- or an anisotropic extended theorie [10] it turned out that the accuracy of the measurement was not high enough to distinguish between these theories.

Fitting the data according to BCS theory one gets a reduced energy gap $\Delta_o/kT_c = 1.85 \pm 0.02$ in the frequency range of 20 to 26 GHz and 1.97 ± 0.04 at 80 to 88 GHz. It seems therefore to be possible, that the energy gap increases with increasing frequency.

On the other hand the measurement of the value $R_s(4.2K) - R_{res}$ at different frequencies may give a distinction of the applicability of the mentioned theories. Fig. 14 shows

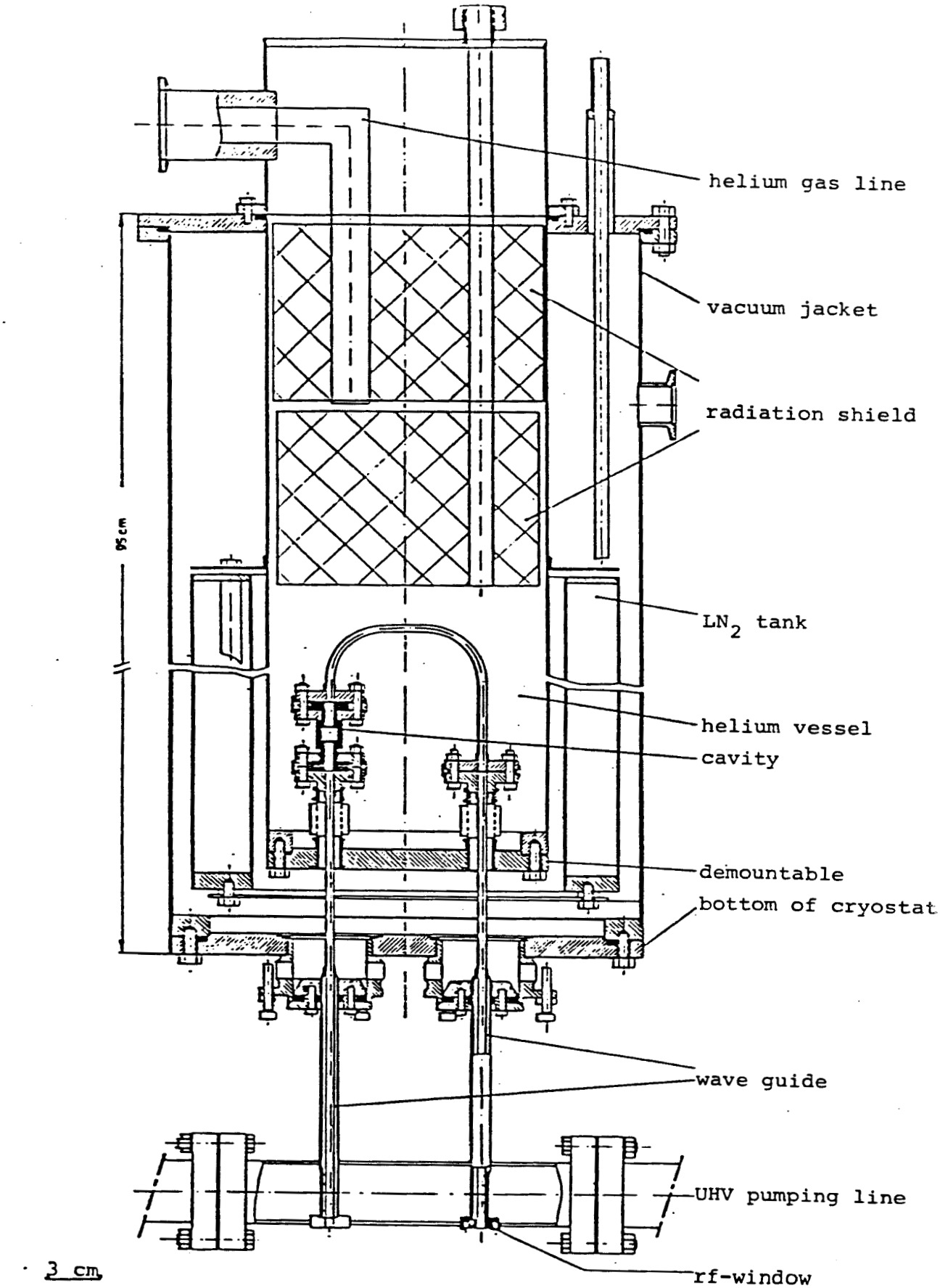

Fig. 13: Experimental setup for testing 80 GHz - cavities

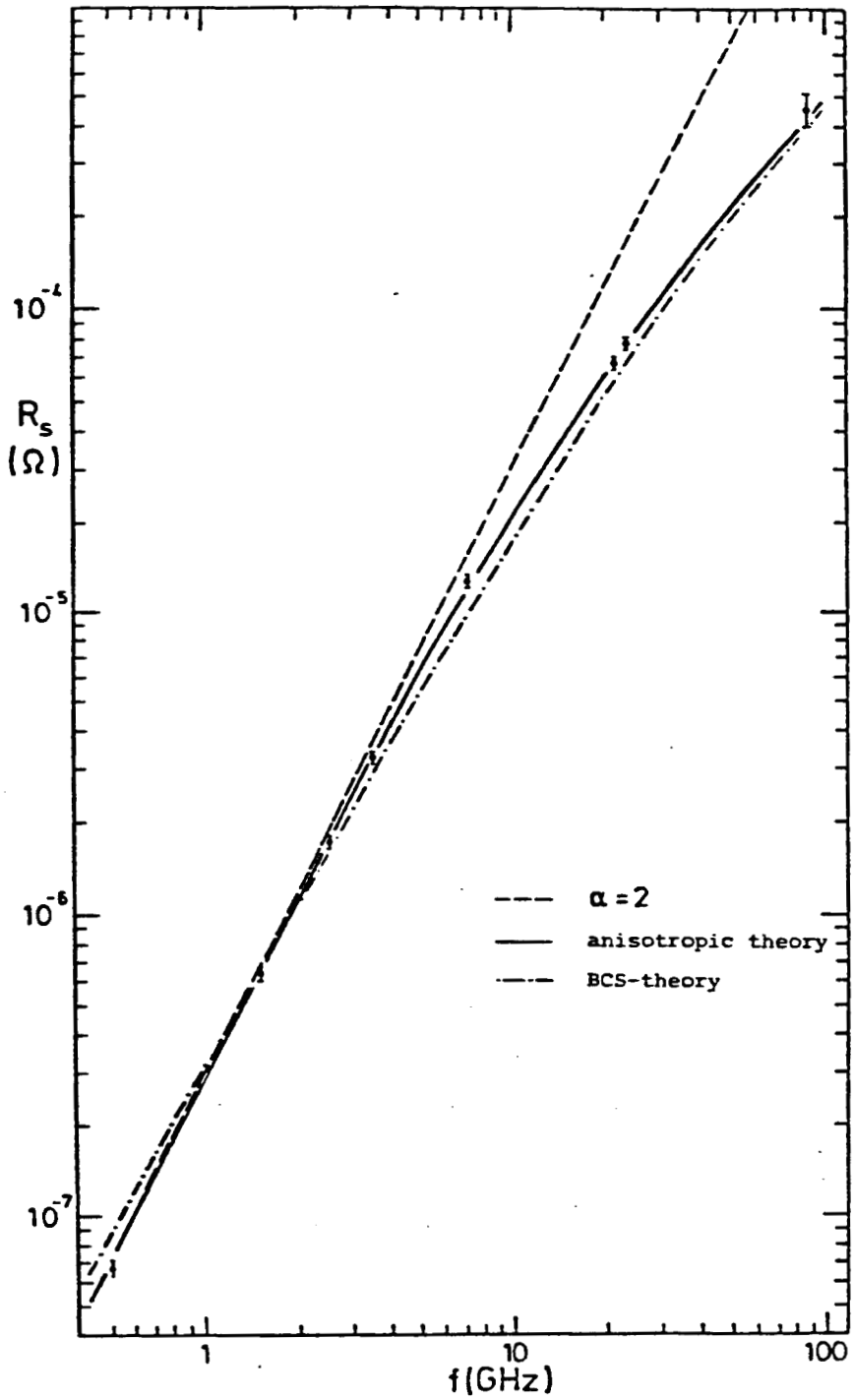

Fig. 14: Frequency dependence of R_s for Nb, $R_s \propto \omega^{\alpha(\omega)}$

the dependence of this value of the frequency. [7,10] It seems that the anisotropic theory fits the experimental data better than BCS-theory.

Fig. 15 shows the same analysis for Nb_3Sn surfaces [12], the analysis is up to now not finished, therefore the shown data are very preliminary.

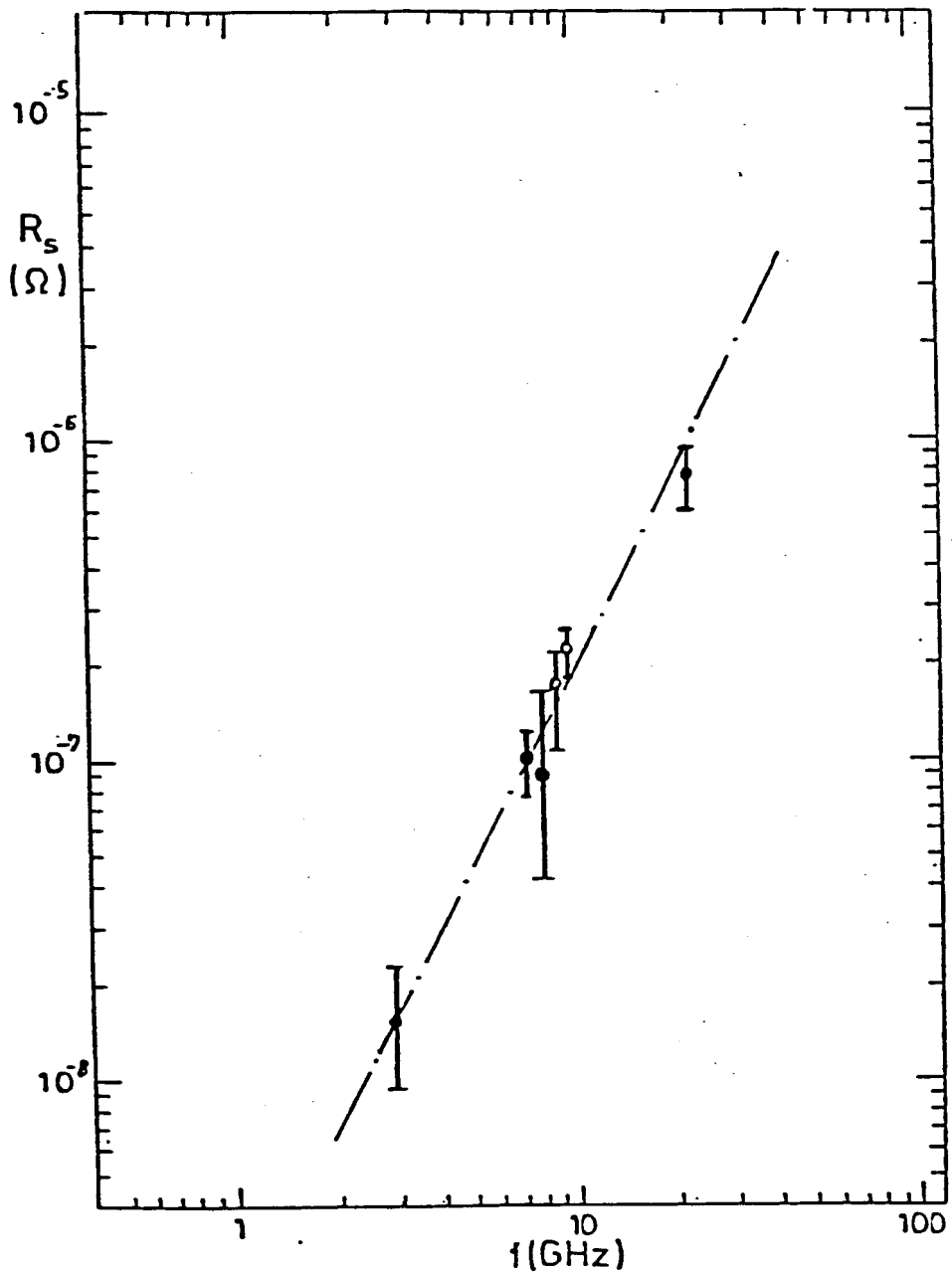

Fig. 15: Frequency dependence of R_s for Nb_3Sn
● measured at Wuppertal
o other laboratories
(very preliminary data) the line indicates
$R_s \propto \omega^2$

Acknowledgment

In this report we have described only one contribution to the Darmstadt superconducting recyclotron. Our colleagues H.Genz, H.D.Gräf, M.Janke, A.Richter, M.Schanz, E.Spamer and O. Tietze of the Institut für Kernphysik der TH Darmstadt carry the responsibility for the construction of this accelerator. We would like to thank them for the opportunity of this collaboration between two university laboratories.

In the field of developing accelerating structures we like to appreciate highly our fruitful collaborations with CERN and DESY. It is not only their technical and financial support which helps us but also the fruitful and stimulating discussions of the results which we can have with our colleagues in these two laboratories. We would like to thank especially Ph.Bernard and H.Lengeler from CERN and G.A.Voss and D.Proch from DESY.

Finally we like to acknowledge gratefully the support of the Deutsche Forschungsgemeinschaft and the Ministerium für Wissenschaft und Forschung des Landes Nordrhein Westfalen.

References

1 H.Heinrichs et al., Proc. of the Conf. on Nuclear Physics with Electromagnetic Interactions (1979) Lecture Notes in Physics 108 p. 176

2 T.Grundey, thesis BUGH-Wuppertal 1983

3 T.Grundeay, priv. communication

4 H.Piel, Proc. Workshop on RF-Superconductivity, Karlsruhe KfK-3019 (1980)

5 T.Grundey, et al., Nucl. Instr. Meth. 224 (1984) p.5-16

6 G.Müller, Diagnostic Technique and Defect Classification, this Workshop

7 U.Klein, thesis BUGH-Wuppertal 1981

8 M.Peiniger, Diplomarbeit BUGH-Wuppertal 1983

9 G.Arnolds-Mayer, A-15 Surfaces in Nb Cavities, this Workshop

10 G.Müller, thesis BUGH-Wuppertal 1983

11 M.Peiniger, priv. communication